Spectroscopic studies of cryogenic fluids: Benzene in propane

R. Nowak and E. R. Bernstein

Spectroscopic studies of cryogenic fluids: Benzene in propane[a]

R. Nowak[b] and E. R. Bernstein

Department of Chemistry, Condensed Matter Sciences Laboratory, Colorado State University, Fort Collins, Colorado 80523

Energy shifts and bandwidths for the $^1B_{2u} \leftrightarrow {}^1A_{1g}$ optical absorption and emission transitions of benzene dissolved in propane are presented as a function of pressure, temperature, and density. Both absorption and emission spectra exhibit shifts to lower energy as a function of density, whereas no shifts are observed if density is kept constant and temperature and pressure are varied simultaneously. Density is thus the fundamental microscopic parameter for energy shifts of optical transitions. The emission half-width is a linear function of both temperature and pressure but the absorption half-width is dependent only upon pressure. These results are interpreted qualitatively in terms of changes occurring in the intermolecular potentials of the ground and excited states. Both changes in shape of and separation between the ground and excited state potentials are considered as a function of density. Classical dielectric (Onsager–Böttcher), microscopic dielectric (Wertheim) and microscopic quantum statistical mechanical (Schweizer–Chandler) theories of solvent effects on solute electronic spectra are compared with the experimental results. Calculations suggest limited applicability of dielectric theories but good agreement between experiment and microscopic theory. The results demonstrate the usefulness of cryogenic solutions for high pressure, low temperature spectroscopic studies of liquids.

I. INTRODUCTION

Optical spectroscopic studies of liquid solutions are confronted with two problems: large spectral linewidths and congestion due to hot bands. These problems have to some extent been overcome by employing low temperature cryogenic liquids (i.e., N_2, CO, O_2, NF_3, CH_4, C_2H_6, C_3H_8, etc.) as solvents; these liquids have proven to be good solvents yielding well resolved, relatively sharp (for the liquid phase) emission and absorption spectra of simple aromatic molecules.[1-7] Optical spectroscopic studies of aromatic solute molecules in simple cryogenic liquids have been used to elucidate microscopic properties of liquid solutions, including an estimate of the solute–solvent intermolecular potentials.[3,5] These studies have focused on the comparison of different solute–solvent systems in terms of gas to liquid transition energy shifts, bandwidths, fluorescence and phosphorescence lifetimes, solubilities, aggregate formation, and their temperature dependences.

Most of the existing theories which treat solvent effects on solute electronic spectra have been based on second order quantum mechanical perturbation calculations of the solute–solvent dipolar intermolecular coupling.[8-11] The classical nonpolar solvent shift theories[10,11] correlate spectral transition energy shift with the macroscopic solvent optical dielectric constant (refractive index) but do not relate spectral behavior directly with any microscopic parameters.

Schweizer and Chandler (S–C)[12] have recently developed a quantum statistical mechanical perturbation theory which relates the solute transition energy shift to the solution density and the polarizabilities of the solute and solvent molecules. The important conclusion of this theory is that the relative solute transition energy shifts are an essential

function of the solvent isothermal microscopic density. The theory also predicts that the solute spectral shifts will depend on the detailed structure of the solvent and on solvent fluctuations. The validity of this approach has been discussed by its authors[12] based on a limited data set obtained at 300 K.[13-15]

The relative solute transition energy shifts calculated as a function of density are significantly different for dielectric and microscopic (quantum statistical mechanical) theories.[12] Additional detailed experiments and calculations are needed to elucidate quantitatively the deviations from dielectric theories and the applicability of the microscopic treatment. Traditionally, experiments have focused on variable solvent and isothermal density studies[13-16]; more definitive tests of the theories would involve variable density (temperature and pressure dependent) studies. Employing both temperature and pressure changes for density variations, one should be able, in principle, to separate potential and kinetic energy increments to the total spectral behavior.

Cryogenic liquid systems are ideal for the above studies because they provide relatively sharp, well resolved solute spectroscopic features which can be obtained over a wide range of pressures and low temperatures. Thus, relatively large density variations can be achieved for these systems without resorting to excessively high pressures.

In this paper we report the results of optical spectroscopic studies and theoretical calculations for benzene dissolved in liquid propane. Propane has been chosen for the initial studies for a number of reasons. First, spectroscopic behavior of different organic molecules (e.g., benzene, naphthalene, toluene, and pyrazine) in propane at low temperature and atmospheric pressure is well known from our previous work.[1-7] Second, propane has well established solvation properties with respect to benzene; no aggregates are found for benzene/propane solutions. Third, propane is a good liquid pressurizing medium: it has a high critical tem-

perature (369.85 K) and low critical pressure (4.247 MPa) and well known thermodynamic data. Both pressure and temperature dependences of the density and dielectric constant[17–19] are available: these data are important for setting up experimental conditions and for performing theoretical calculations.

Moreover, benzene has previously proved to be a good solute molecule for the probing of liquid state interactions and structure.[1,3,4] Benzene has high symmetry, well known spectra and relaxation dynamics, and good solubility. The intense vibronic series $6_0^1 1_0^n$ and $6_1^0 1_n^0$, $n = 0,1,2,3,...$ of the benzene $^1B_{2u} \leftrightarrow ^1A_{1g}$ transition can be observed in both absorption and emission and can be readily followed as a function of temperature and pressure in liquid propane.

The well resolved absorption and emission spectra of benzene in liquid propane are determined as a function of the theoretically important parameters temperature, pressure, and density. Comparing both absorption and emission behavior, we are able to estimate changes in the intermolecular potential surfaces in both the ground and excited electronic states. To the best of our knowledge this is the first report of electronic emission spectra in a solute–solvent system as a function of pressure. The comparison of the experimental data with dielectric and microscopic theories demonstrates the limited applicability of dielectric theories and the accuracy of the microscopic quantum statistical mechanical treatment.

II. EXPERIMENTAL PROCEDURES

The optical absorption and dispersed emission spectra of the benzene $^1B_{2u} \leftrightarrow ^1A_{1g}$ transition are studied as a function of pressure, temperature, and density in the ranges 0–3 kbar, 90–200 K, and 640–755 kg m^{-3}, respectively. The experiments consist of constant pressure, variable temperature, constant temperature, variable pressure, and simultaneous variable pressure and temperature studies of transition energies and bandwidths.

Most of the experimental setup, with the exception of the high pressure cell and pressurizing system, is analogous to the one described elsewhere.[1–3] A conventional UV xenon lamp and pulsed Nd^{+3}/YAG pumped dye (LDS 698) laser, whose output is frequency doubled and mixed with the 1.064 μm fundamental of the YAG laser, are used as light sources for absorption and emission, respectively. A 1 m monochromator with a 2400 groove/mm holographic grating is used to disperse both absorption and emission. Absorption is detected with photon counting electronics and emission is recorded with a boxcar averager and a computer. Sample temperature is controlled by a mechanical refrigerator.

The sample is maintained at the desired pressure and temperature in a right circular cylindrical cell with a 1 cm^3 volume and a 1.2 cm absorption pathlength. The cell has four cone-shaped sapphire windows at 90° to one another at the central circumference of the cylinder. All windows have $f/3$ optical access. The windows are sealed to holders with epoxy (Crest 7450). The holders are sealed to the cell by tapered indium coated brass gaskets at the high pressure side, backed by either Teflon or indium packing and indium coated brass gaskets at the low pressure side. The cell oper-

ates in the pressure range from 10^{-6} Torr to 4 kbar at temperatures from 70 to 300 K without the need for frequent packing replacement. The pressurizing system consists of hand operated generators and valves (High Pressure Equipment Corp.) and is connected to a high vacuum pumping system. Pressure is measured by resistance pressure transducers (Sensotec) to an accuracy of $\pm$ 20 bar.

All chemicals are obtained in the highest available commercial purity and used without additional purification. Gas samples for deposit in the precooled cell are prepared by mixing solute and solvent at room temperature. Benzene concentration (typically 50–200 ppm) is controlled by temperature variation of its vapor pressure in a known volume. The entire system is filled with this mixture or pure propane which acts as the pressurizing fluid. The number of benzene molecules in the optical path changes by about 20% due to the density change over the course of the experiment. Additionally, the solubility of benzene in propane is both temperature and pressure dependent. These effects are in part responsible for the apparent change in transition intensity with pressure. We assume that these concentration changes are not important for the interpretation of transition energy shifts and transition half-widths; however, they do obscure comparison of the absolute and relative intensities of the features at different experimental conditions.

III. THEORY OF SOLVENT EFFECTS ON SOLUTE ELECTRONIC SPECTRA

The following presentation is limited only to those theoretical results which are pertinent to the interpretation of our experimental energy shifts. Specifically, results of the Onsager–Bottcher (O–B) and Wertheim (W) dielectric models, and the results of the quantum statistical mechanical theory of Schweizer and Chandler (S–C) will be outlined.

A. Classical dielectric theories

As a rule, all dielectric theories relate the absorption energy shift of a solute impurity molecule dissolved in a nonpolar liquid to the static solvent dielectric constant (refractive index). The predictions of such a theory are uniquely fixed once the solvent dielectric constant is specified. Dielectric models differ among themselves in the constraints imposed on the local electric field acting on the solute molecule generated by the surrounding liquid continuum. The absorption energy shift predicted by dielectric models is expressed, in general, by[10]

$$\Delta\omega = \frac{-e^2 f_0}{2m\omega_0} \left(\frac{b}{1 - b\alpha_b} \right) \tag{1}$$

in which f_0 is the oscillator strength of the electronic transition taking place at a frequency ω_0, e and m are electron charge and mass, respectively, α_b is the background contribution to the isolated solute molecule polarizability, and b is the factor associated with the "reaction field," i.e., the field due to polarization of the surroundings by the solute induced dipole moment. For specific O–B[10,20] and W[10,21] local field models, $b = R_u^{-3}[2(\epsilon - 1)/(2\epsilon + 1)]$ and $b = 16\xi R_u^{-3}$, respectively, in which R_u is a density independent constant (the solute cavity radius). Explicit expressions of Eq. (1) for

the absorption energy shift in the O–B and W models are

$$\text{O–B:} \quad \Delta\omega = k \left(\frac{n_b^2 + 2}{3}\right) \left(\frac{\epsilon - 1}{2\epsilon + n_b^2}\right) \quad (2)$$

and

$$\text{W:} \quad \Delta\omega = k \frac{8\xi}{1 - 16\xi\alpha_b R_u^{-3}} . \quad (3)$$

In the above equations the proportionality constant $k = -e^2 f_0 / m\omega_0 R_u^3$, n_b is the "internal" solute refractive index defined as $(n_b^2 - 1)/(n_b^2 + 2) = \alpha_b R_u^{-3}$, and ξ is the parameter related to the solvent dielectric constant, as calculated in the mean spherical approximation[21] (MSA). ξ is found by the relation

$$\epsilon = \frac{(1 + 4\xi)^2 (1 + \xi)^4}{(1 - 2\xi)^6} . \quad (4)$$

Equations (2) and (3) predict red energy shifts with increasing dielectric constant (presumably associated with the increase of solvent density), the shift being slightly larger for the W model than for the O–B model.[10] Quantitative comparison between experiment and dielectric theories hinges on the determination of parameters R_u and α_b, which cannot be specified unambiguously. Although R_u is theoretically a density independent constant, some workers[13–15] have assumed R_u^{-3} proportional to the density in order to obtain better agreement with experiment. Due to the difficulties with the specification of α_b, one usually assumes that $\alpha_b = 0(n_b^2 = 1)$. Instead of using Eqs. (2) and (3), their following simplified versions are used:

$$\text{O–B:} \quad \Delta\omega = k \frac{(\epsilon - 1)}{(2\epsilon + 1)}, \quad (5)$$

$$\text{W:} \quad \Delta\omega = 8k\xi. \quad (6)$$

Within this approach, Eq. (5) resembles the classical result of Bayliss.[11(a)] The existing literature data indicate that in the few cases studied, dielectric theories give a correct qualitative prediction of the shifts; however, in order to obtain more quantitative agreement between the theory and experiment, additional assumptions concerning proportionality constants (R_u in particular) must be made.[13–15]

B. Microscopic quantum statistical mechanical theory

The basic assumptions of the microscopic (S–C) theory[12] of solvent perturbations of solute electronic spectra are (1) the fluctuating single molecule quantum mechanical point dipole is approximated by a two parameter harmonic oscillator (Drude) model, (2) fluctuating dipoles of both solute and solvent molecules interact via induced dipole–induced dipole and solute induced dipole–solvent permanent dipole coupling, and (3) the solvent is considered to be a fluid composed of spherical molecules interacting via long range attractions and short range hard sphere repulsions (in the sense of the MSA[21]). The principal result of the theory is an exact analytical expression relating the absorption transition energy shift to the microscopic density and the solute and solvent polarizabilities. Under the assumption that the solute absorption energy in the gas phase ($\omega_{0,I}$) is far re-

moved from a solvent absorption band (ω_0), the frequency shift of the solute electronic transition is given by[12]

$$\Delta\omega = \omega_{0,I}\{1 - 2\alpha_{0,I}E'[\alpha'(\omega_{0,I})]\}^{1/2} - \omega_{0,I}$$

$$\simeq \omega_{0,I}\alpha_{0,I}E'[\alpha'(\omega_{0,I})] \quad (7)$$

in which $\alpha_{0,I}$ is the isolated solute molecule (real) polarizability, $\alpha'(\omega_{0,I})$ is the real part of the single solvent molecule complex polarizability taken at the frequency $\omega_{0,I}$ [see Eq. (11) below], and $E'(\alpha')$ is generally a function describing the modification of the isolated molecule polarizability due to interparticle coupling in solution. The results of the theory should not depend on the specific form of $E'(\alpha')$; however, typically the standard Padé form is used[22]:

$$E'[\alpha'(\omega_{0,I})] = a\alpha'(\omega_{0,I})/[1 + b\alpha'(\omega_{0,I})] \quad (8)$$

in which the coefficients a and b are functions of both density (ρ) and temperature and can be determined from the properties of the dipolar hard sphere fluid.[23] Such a procedure yields[12]

$$a = 4\pi\rho\sigma^{-3}I_2(\rho\sigma^3), \quad (9)$$

$$a/b = E_\infty = 4\pi^2\sigma^{-3}I_2^2(\rho\sigma^3)/I_3(\rho\sigma^3) \quad (10)$$

in which the numerical functions $I_2(\rho\sigma^3)$ and $I_3(\rho\sigma^3)$ are given below by Eqs. (17) and (18), and σ is the hard sphere diameter in the sense of the MSA. $\alpha'(\omega_{0,I})$ in Eqs. (7) and (8) can be obtained by deriving the real part of the single solvent molecule complex polarizability from Eq. (7) of Ref. 22:

$$\alpha'(\omega_{0,I}) = -\alpha_0[B(\omega_{0,I})/A(\omega_{0,I})]$$

$$\times\{1 - [1 - 2A(\omega_{0,I})/B^2(\omega_{0,I})]^{1/2}\} \quad (11)$$

in which the functions $A(\omega_{0,I})$ and $B(\omega_{0,I})$ are

$$A(\omega_{0,I}) = 2\alpha_0 b [(\omega_{0,I}/\omega_0)^2 - 1 + 2\alpha_0 E_\infty], \quad (12)$$

$$B(\omega_{0,I}) = (\omega_{0,I}/\omega_0)^2 - 1 + \alpha_0 b. \quad (13)$$

By using Eqs. (7)–(13), one can obtain an explicit form for the relative energy shift $\Gamma = \Delta\omega/\omega_{0,I}$ as a function of the four dimensionless parameters $\rho\sigma^3$, α_0/σ^3, $\alpha_{0,I}/\sigma^3$, and $\omega_{0,I}/\omega_0$:

$$\Gamma = \frac{\dfrac{2\pi^2 \alpha_{0,I} I_2^2(\rho\sigma^3) X}{\sigma^3 I_3(\rho\sigma^3) Y} \left\{1 - \left[1 - \dfrac{4\rho\sigma^3 \alpha_0 I_3(\rho\sigma^3) Y}{\pi\sigma^3 I_2(\rho\sigma^3) X^2}\right]^{1/2}\right\}}{1 - \dfrac{X}{2Y}\left\{1 - \left[1 - \dfrac{4\rho\sigma^3 \alpha_0 I_3(\rho\sigma^3) Y}{\pi\sigma^3 I_2(\rho\sigma^3) X^2}\right]^{1/2}\right\}} \quad (14)$$

with

$$X = (\omega_{0,I}/\omega_0)^2 - 1 + \frac{\alpha_0}{\sigma^3}\rho\sigma^3 \frac{I_3(\rho\sigma^3)}{\pi I_2(\rho\sigma^3)}, \quad (15)$$

$$Y = 8\pi^2 \frac{\alpha_0 I_2^2(\rho\sigma^3)}{\sigma^3 I_3(\rho\sigma^3)} . \quad (16)$$

Numerical functions $I_2(\rho\sigma^3)$ and $I_3(\rho\sigma^3)$ are calculated explicitly[24]:

$$I_2(\rho\sigma^3) = \frac{1}{3} \left\{ \frac{1 - 0.3618\rho\sigma^3 - 0.3205(\rho\sigma^3)^2 + 0.1078(\rho\sigma^3)^3}{(1 - 0.5236\rho\sigma^3)^2} \right\}, \tag{17}$$

$$I_3(\rho\sigma^3) = \frac{2.741\,46}{2.707\,96} \left\{ \frac{2.707\,97 + 1.689\,18\rho\sigma^3 - 0.315\,7(\rho\sigma^3)^2}{1 - 0.590\,56\rho\sigma^3 + 0.200\,59(\rho\sigma^3)^2} \right\}. \tag{18}$$

Equation (14) predicts the relative energy shift for solute absorption as a function of density, solute and solvent polarizabilities, and absorption band energies. The equation allows one to reproduce the results of the model calculations of the S–C theory.[12]

The derived dependence of the solute transition shift on the microscopic parameters can be explored by performing high pressure, density dependent experiments for different solute–solvent systems. Most of the experimental investigations of the solute transition energy shift as a function of molecular environment have involved variable solvent studies. A cleaner and more definitive test of the theory should be obtained by applying high pressures and low temperatures as a tool to vary the solute environment.

IV. EXPERIMENTAL RESULTS

Using the high pressure optical cell described above, we are able to reproduce all the previously reported results for the benzene/propane system at atmospheric pressure.[1,3] New results obtained as a function of temperature, pressure, and density are reported in this section. As all the bands in either absorption or emission spectra respond to perturbations in the same manner, only the representative behavior for the 6_0^1 and 6_1^0 bands of the $^1B_{2u} \leftrightarrow {}^1A_{1g}$ transition of benzene is discussed.

Figures 1(a) and 1(b) show the typical pressure development of the absorption and emission spectra, together with the spectra taken at different temperatures. As can be seen from the dependence summarized in Fig. 2, both absorption and emission spectra are red shifted with increasing pressure at constant temperature, that is, with an increase of isothermal density. The pressure dependences are linear (− 20 to − 30 cm^{-1}/kbar) and slightly temperature dependent. The pressure dependences for emission seem to be slightly steeper than the corresponding dependences for absorption, but the magnitude of this effect is within experimental error. The absolute energy shifts as a function of pressure are relatively small compared to the experimental error (∼15–20 cm^{-1}). This error results primarily from the uncertainty in the determination of band maxima due to relatively large band half-widths (∼160 cm^{-1} for absorption and ∼200 cm^{-1} for emission).

Both absorption and emission spectra are slightly blue shifted with increasing temperature at constant pressure, that is, with decreasing isobaric density (see Fig. 3). The slopes of these linear dependences are ∼45 cm^{-1}/100 K for absorption and ∼60 cm^{-1}/100 K for emission. Similar dependences were observed in our previous experiments at atmospheric pressure but not reported because of their small size.

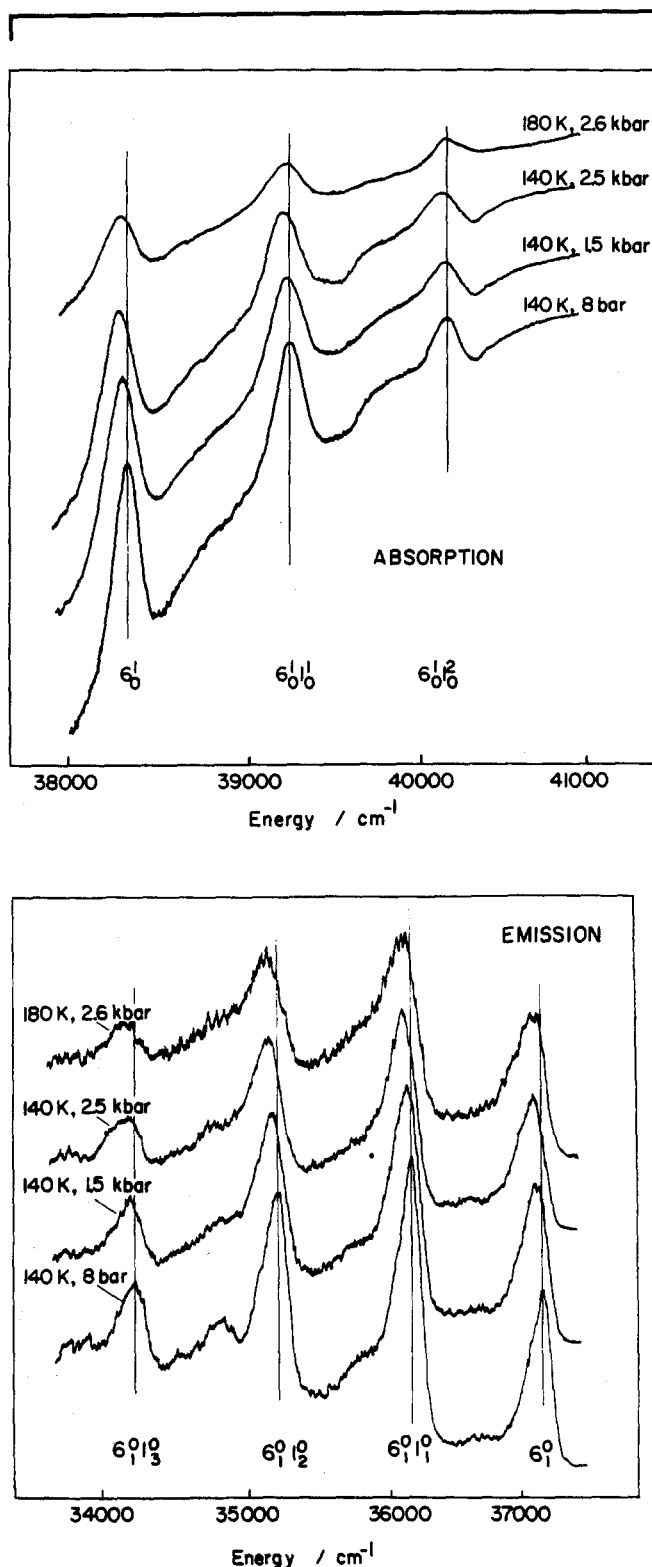The shifts of both absorption and emission spectra can

FIG. 1. Typical pressure and temperature development of absorption (a) and emission (b) spectra of ∼150 ppm of benzene in propane. Note transition energy shifts to the red and band broadening as a function of pressure and temperature.
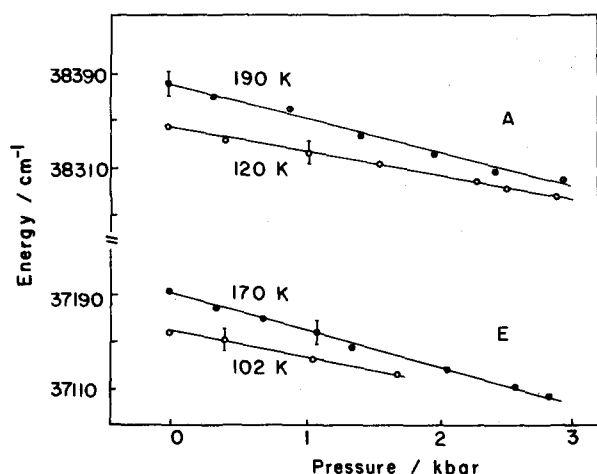
FIG. 2. Pressure dependence of the 6_0^1 and 6_1^0 band energies for absorption (A) and emission (E), taken at different temperatures. The dependence at 102 K is not studied at higher pressures due to solidification of propane.

FIG. 4. Absorption (A) and emission (E) transition energy shifts plotted as a function of experimental density (calculated from thermodynamic data). Different points correspond to various experimental runs performed either as a function of pressure at constant temperature or as a function of temperature at constant pressure.

be expressed as a function of experimental density (calculated from thermodynamic data)[19] by plotting the energy shifts obtained from different experiments on the same graph. The result given in Fig. 4 shows that the transition energy is a fairly linear function of density. The slope of this dependence is $\sim -80 \, \text{cm}^{-1}/100 \, \text{kg}^{-3}$, both for absorption and emission. The error bars in Fig. 4 reflect the experimental uncertainty between different experiments performed either as a function of pressure or temperature. The observation that all the experimental points fit fairly well to a linear dependence suggests that the density (microscopic intermolecular distance) is the main parameter governing the solute spectral shifts. This is proven by performing experiments at constant density through simultaneous variation of temperature and pressure. Absorption and emission spectra taken at constant density (Fig. 5) do not exhibit any pronounced shifts, even though temperature and pressure are widely varied. A small tendency for a red shift (see Fig. 5), at most $\sim -20 \, \text{cm}^{-1}$ for a 100 K change of temperature and simultaneous 3 kbar change of pressure, falls entirely within the experimental uncertainty. Absence of an energy

shift at constant density arises from the compensation of opposite temperature and pressure effects on the transition energy (compare Figs. 2 and 3) and demonstrates clearly the fundamental microscopic nature of the density. This new experimental finding is of a great importance to the theory.

Temperature and pressure dependences of the bandwidths are given in Figs. 6 and 7. Absorption half-widths increase with pressure but are temperature independent, whereas those for emission exhibit asymmetric red-shaded broadening with both temperature and pressure. In general, the increase of bandwidth with temperature is predominantly caused by the increase of the kinetic energy and concomitant change in the equilibrium population of the states. Absence of broadening for absorption and asymmetric red-shaded broadening for emission with increasing temperature have already been explained in the literature[3] on
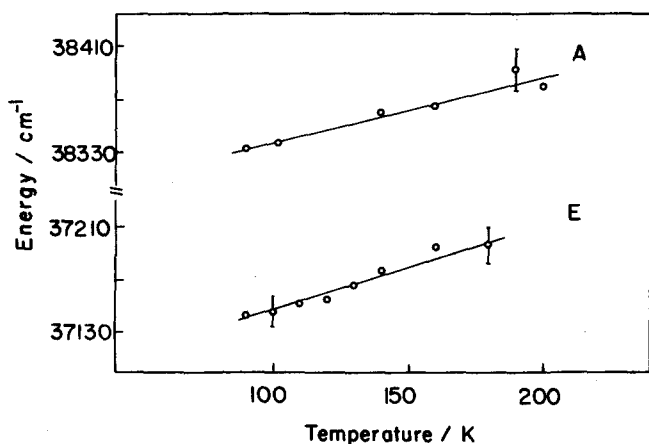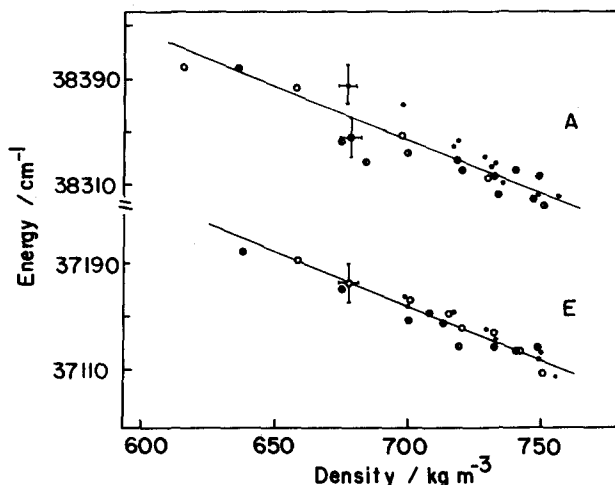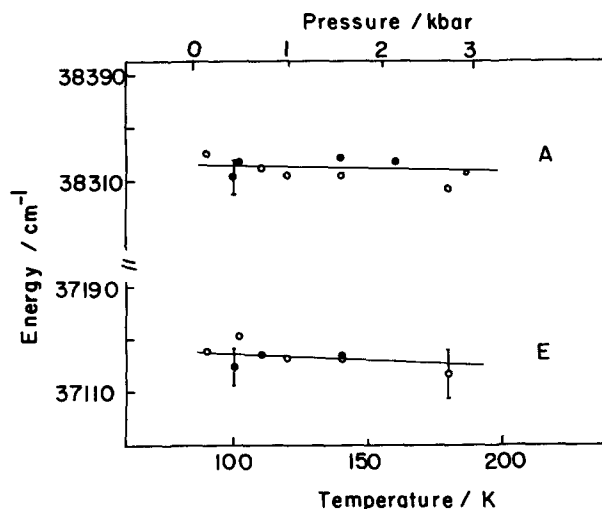

FIG. 3. Temperature dependence of the 6_0^1 and 6_1^0 band energies for absorption (A) and emission (E), taken at constant low pressure of 9 bar.

FIG. 5. Transition energies for absorption (A) and emission (E) measured at constant density $\rho = 730 \, \text{kg m}^{-1}$ as a function of simultaneously varied temperature and pressure. Similar dependences are recorded at density $\rho = 700 \, \text{kg m}^{-1}$.
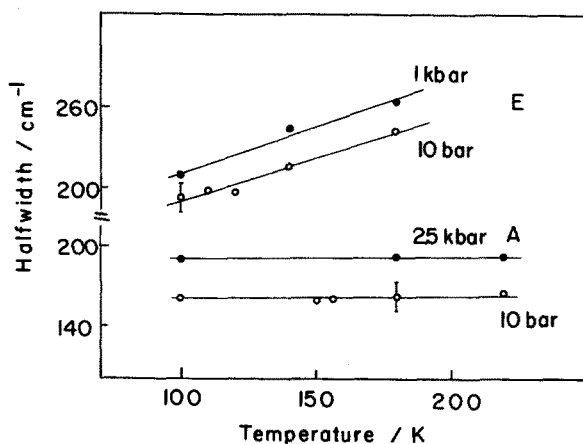
FIG. 6. Temperature dependences of the absorption 6_0^1 band (A) and emission 6_1^0 band (E) half-widths at different pressures.

different relative equilibrium positions for the ground and excited state intermolecular potential surfaces and their different slopes for the repulsive and attractive parts of the potential. The pressure induced changes in bandwidths and differences between the absorption and emission behavior will be discussed in the following section.

The intensities of both absorption and emission change considerably with pressure and temperature. Most of the intensity change is due to either changes of concentration (solubility) or density (number of benzene molecules in the cell). Both these effects seem to be important; however, the observation that the emission intensity decreases more rapidly under the same experimental conditions than the absorption intensity suggests an additional quenching of fluorescence at high pressures. Perhaps at high pressures other nonradiative decay channels can be accessed (e.g., intersystem crossing) which can be responsible for the decrease in the emission intensity. The $^1B_{2u}$ state of benzene may in addition relax through a high-efficiency nonradiative pathway accessible at energies ~ 2500 cm^{-1} above the zero point energy of the $^1B_{2u}$ state.[25-27] Although this route may be open
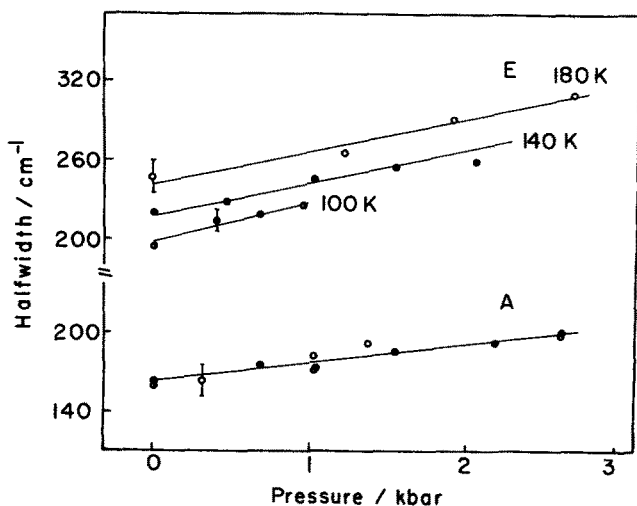

FIG. 7. Pressure dependences of the absorption 6_0^1 band (A) and emission 6_1^0 band (E) half-widths at different temperatures.

to benzene in propane, especially at high pressures, the temperatures in our experiment are not high enough to make this channel very efficient.

V. DISCUSSION

A. Ground and excited state potential surfaces—qualitative explanation of the experiments

Electronic transitions of solvated molecules are different from those of isolated molecules due to the interactions with the surrounding solvent "cage" molecules. The absorption process for benzene in solution can be regarded as an electronic excitation from the ground state equilibrium configuration ($^1A_{1g}$ in the minimum energy solvent cage configuration at a given temperature) to the excited Franck–Condon state configuration ($^1B_{2u}$ in the same solvent configuration cage) as depicted in Fig. 8. The excited Franck–Condon state relaxes to the excited equilibrium state due to the fast (of the order of 10^{-12}–10^{-11} s) solvent and intramolecular vibrational relaxation. In a like manner, the final state resulting from emission from the excited equilibrium configuration is the Franck–Condon and not the equilibrium ground state configuration. This Franck–Condon state subsequently relaxes to the ground equilibrium state on a time scale of 10^{-12}–10^{-11} s. We have previously suggested[3] that the minimum of the excited state potential surface lies at a smaller intermolecular distance (r_e) than the corresponding minimum of the ground state surface located at a distance r_g. As a result, the Franck–Condon por-
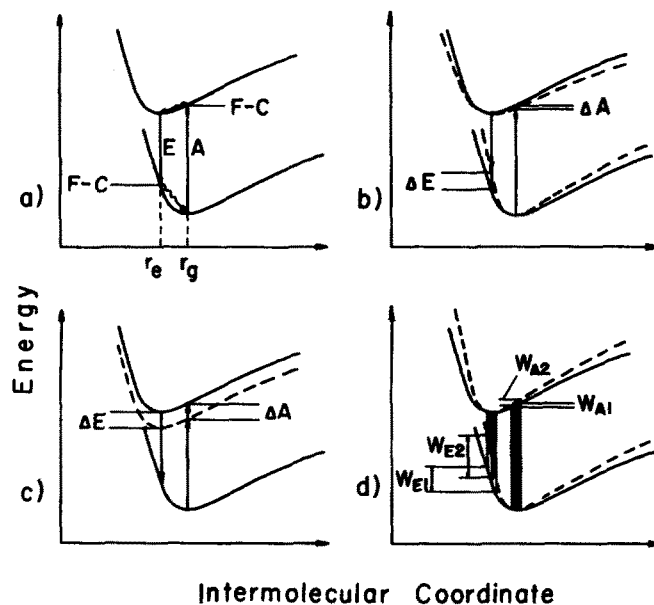

Intermolecular Coordinate

FIG. 8. Diagrams of the intermolecular potential energy as a function of averaged intermolecular coordinate. A and E correspond to absorption and emission processes, respectively. r_g and r_e are the equilibrium intermolecular coordinates of the minimum potential energy in the ground and excited state, respectively. F–C stands for the Franck–Condon state accessed by either absorption or emission. The ground and excited state potential surfaces are assumed to be identical. The dotted lines represent the possible changes of the potential surfaces discussed in the text. ΔA and ΔE represent anticipated transition energy shifts for absorption and emission induced by the changes in the intermolecular potential. ($W_{A2} - W_{A1}$) and ($W_{E2} - W_{E1}$) correspond to changes in band half-widths induced by pressure.

tion of the upper potential accessed by absorption is less steep than the Franck–Condon portion of the ground state potential accessed by emission. Such a shift of the average equilibrium intermolecular potentials between excited and ground states is consistent with the expanded size and polarizability of the benzene molecule in the excited state.[28] The situation described above and depicted in Fig. 8(a) accounts for emission line broadening as a function of temperature at atmospheric pressure and lack of such a broadening for absorption; however, it does not explain the transition energy shifts and broadening observed experimentally as a function of pressure.

Changes in the potential surfaces occurring as both temperature and pressure are varied are obviously more complex. In principle, changing pressure and/or temperature may have three different effects on the intermolecular potential surfaces of the ground and excited states. First, the separation distance $(r_g - r_e)$ between the energy minima in the ground and excited state may change. Second, the shapes of the repulsive and attractive parts of both ground and excited state potential surfaces may vary due to pressure and temperature (density) induced changes in the interactions. Third, the change in interactions due, for example, to different variations of solvation energies in the ground and excited states may change the energy gap between the ground and excited state potential surfaces. In practice, one would expect all the three effects to take place simultaneously; however, some of these effects are argued below to be of less importance than the others.

Pressure and temperature dependences of the energy shifts can be expressed uniquely as a function of density. Within this simplified assumption, only density effects on the potential surfaces and energy shifts can be analyzed. Note (Fig. 4) that the energy shifts as a function of density are to the red and of a similar magnitude for both absorption and emission.

Consider now each of the three abovementioned possibilities for changing the intermoleuclar solute–solvent potentials:

(1) Increase of the relative separation distance $(r_g - r_e)$ between the minima of the ground and excited state potential surfaces as a function of density [see Fig. 8(a)] would cause a relative emission energy shift to the red; absorption, however, would have to be shifted simultaneously to the blue. Decrease of the $(r_g - r_e)$ distance would cause exactly the opposite effect, shifting the emission spectrum to the blue and absorption spectrum to the red. Neither of these effects is observed experimentally.

(2) If both repulsive and attractive parts of the excited state potential would become relatively less steep, compared to the respective parts of the ground state potential [Fig. 8(b)], both absorption and emission spectra would shift to the red in agreement with the experimental observations. This mechanism, however, seems unlikely to be dominant because the shapes of both the attractive and repulsive parts of the potential would need to change in a similar manner (similar energy shifts for absorption and emission are observed) and the changes of the potential surfaces in the ground and excited states would need to be different and

such that the interaction with the surroundings in the excited state must be weaker than in the ground state. This contradicts the notion that the excited benzene molecule interacts more strongly with its surrounding than does the ground state molecule.

(3) The change in the energy separation between the ground and excited state potential surfaces can lead to either identical red or blue energy shifts of both absorption and emission spectra. Red shifts would obtain if the energy gap between the ground and excited state potential surfaces were inversely proportional to the density [Fig. 8(c)]. Such behavior would account for both the red shift of absorption and emission spectra with increasing of pressure at constant temperature (increase of density) and practically no shift of absorption and emission at constant density (simultaneous changes of both temperature and pressure). In practice, some small differences in slopes of the different dependences for absorption and emission exist (compare Figs. 2 and 3), which cannot be explained by this last mechanism; however, the other two mechanisms (in particular, a small change in the separation distance between the ground and excited states energy minima) can entirely account for these differences. As the magnitude of these latter small effects is of the order of experimental error, the above analysis cannot be more detailed.

The absorption spectral half-widths are temperature independent whereas the emission half-widths increase asymmetrically to the red with increasing temperature. The different behavior for absorption and emission is explained by the relative shift of the ground and excited state potential surface minima [see Fig. 8(a)] and has already been discussed in detail.[3] The broadening of the absorption and emission half-widths as a function of pressure at a constant temperature (Fig. 7) is more difficult to explain because at a constant temperature the equilibrium Boltzmann distribution of states in the ground and excited electronic states does not change (kinetic energy is constant) and thus only changes of the potential surfaces can be taken into consideration.

Broadening of the absorption bands can be explained assuming that the attractive part of the excited state potential surface becomes steeper with increasing pressure [see Fig. 8(d)]. In a like manner, emission band broadening as a function of increasing pressure can be explained by the change in shape of the repulsive part of the ground state potential accessed by emission [Fig. 8(d)]. The repulsive part of the ground state potential would have to become steeper with increasing pressure in order to account for the broadening of emission at high pressures. The change of the repulsive part of the ground state potential must be larger than the change of the attractive part of the excited state potential because the pressure dependence of the half-widths is stronger for emission than for absorption (see Fig. 7). This result underscores the important role of repulsive interactions due to close particle packing at high densities.

As can be seen from the above considerations of intermolecular potentials for solute ground and excited states, both absorption and emission spectral data can be used, with certain simplifying assumptions, to generate useful informa-

tion concerning the microscopic behavior of the benzene/propane system. Insight into the intermolecular interactions and their changes induced by the changes of pressure, temperature, and density can be obtained. One should remember, however, that the description presented here is rather qualitative in comparison with the real, more complex behavior. For example, changes in the intermolecular potentials which we have proposed above to account for band broadenings have an impact on energy shifts and changes of the potential surfaces responsible for the energy shifts may have some influence on the bandwidths. In practice, all these effects take place simultaneously but, as we have shown, some of them are considerably more important than others and dominate the overall behavior. In order to distinguish different small variations in the spectral behavior, spectra of even better resolution and spectroscopic detail than the ones presented in this paper would be needed.

B. Comparison between liquid state theory and experiment

1. Dielectric theories—Onsager-Böttcher and Wertheim models

Within the framework of the dielectric theories outlined in Sec. III, absorption energy shifts are calculated using Eq. (5) for the O–B model and Eqs. (4) and (6) for the W model. The solute dependent proportionality constant k has been set to reproduce the experimental gas to liquid frequency shift of -272 cm^{-1} at 100 K and atmospheric pressure. This procedure gives $k = 1375$ cm^{-1} and $k = 1190$ cm^{-1} for the O–B and W models, respectively. The values of k are different, despite the fact that the theory predicts that k should be identical in both models.[10] The discrepancy indicates that the simplified Eqs. (5) and (6) are not very accurate; the errors caused by using them can be estimated from the above difference in the values of k. Densities and dielectric constants at different experimental temperatures and pressures up to 0.8 kbar are found in Ref. 19. At higher pressures, the density is calculated using a parametric equation of state and the dielectric constant is estimated using the Clausius–Mossotti function.[19] The parameter ξ in the Wertheim model is fitted numerically using Eq. (4). For small $y = (\epsilon - 1)/(2\epsilon + 1)$, which corresponds to the conditions of our experiments, ξ can be also calculated using the inverse of Eq. (4) in the form[10]

$$8\xi = y + 17/32y^2 + 509/64y^3 + \cdots. \tag{19}$$

The results of the calculations of the relative energy shifts as a function of normalized density for the O–B and W models are compared to the experimental results in Fig. 9. As can be seen, the two dielectric models do not generate a good fit to the experimental data. In order to obtain quantitative agreement between experiment and theory the calculations for the O–B model are repeated with the assumption that R_u^{-3} is proportional to the density, i.e., $k = k_0 \rho/\rho_0$ in Eq. (5). Surprisingly, this assumption considerably improves agreement of the model with experiment (see Fig. 9); however, this procedure is somewhat arbitrary and does not have well founded theoretical justification.
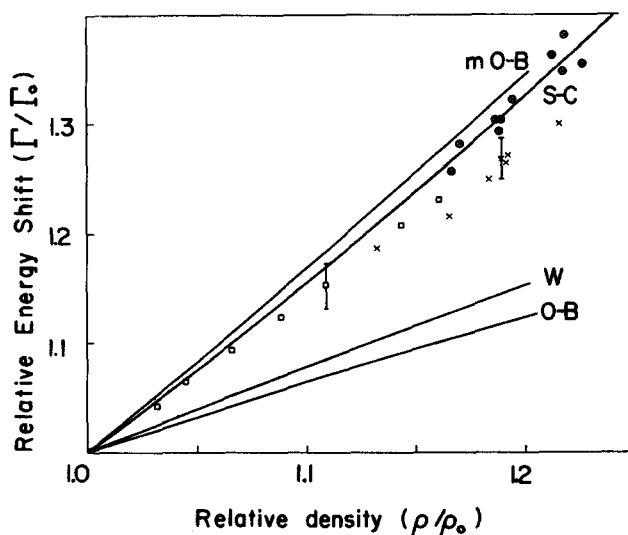

FIG. 9. Relative shift of the absorption 6_0^1 band as a function of normalized density. Differently marked points correspond to various experimental runs. The lines represent the results of calculations for Onsager–Böttcher (O–B), modified O–B (m-O–B), Wertheim (W), and Schweizer–Chandler (S–C) models.

2. Microscopic quantum statistical mechanical model

Numerical implementation of the microscopic S–C theory in the form of Eq. (14) entails specification of four dimensionless parameters: $\rho\sigma^3$, α_0/σ^3, $\alpha_{0,I}/\sigma^3$, and $\omega_{0,I}/\omega_0$. The specific values of the parameters used for calculation are given in Table I. They are choosen as follows: ρ—variable experimental solvent density calculated as a number of molecules per unit volume; α_0—single propane molecule polarizability calculated using bond polarizabilities given in Ref. 29; ω_0—propane electronic transition energy calculated using the value of the first ionization energy ($\hbar\omega_0$) from Ref. 30 (such a choice of α_0 and ω_0 allows one to reproduce London dispersion forces in a liquid); $\alpha_{0,I}$—single benzene molecule polarizability is taken from Ref. 29; $\omega_{0,I}$— benzene gas phase frequency of the 6_0^1 electronic transition; and σ— the hard sphere diameter can be calculated theoretically using Eqs. (48)–(50) of Ref. 21 (according to the MSA procedure) in such a way as to reproduce the experimental density and solvent dielectric constant.

Calculations of the relative shift performed using Eq. (14), with the parameters given in Table I are in a good agreement with the experimental data (see Fig. 9). The calculated absolute value of the gas to liquid shift is, however, ~ -1510 cm^{-1} compared to the experimental value of

TABLE I. Molecular parameters used in the calculations of the S–C theory. Details of the calculations and references for specific parameters are given in the text.

Propane	Benzene
$\epsilon = 1.977\,45$	$\omega_{0,I}$ (cm^{-1}) = 38 638
σ (Å) = 4.7	$\alpha_{0,I}/\sigma^3 = 0.1$
$\alpha_0/\sigma^3 = 0.063$	$\omega_{0,I}/\omega_0 = 0.132$
$\beta\hbar\omega_0 = 953.2$	

$- 272$ cm^{-1}. This discrepancy[12] is presumably due to the use of the two parameter harmonic oscillator model and to the neglect of the existence of many other electronic states with different transition oscillator strengths. One can easily correct the value of the gas to liquid shift by adjusting $\alpha_{0,I}$; this can be done because the frequency shift is a simple linear function of solute polarizability. For benzene in propane this procedure would require that $\alpha_{0,I}$ equals 27 Å^3 instead of 103.2 Å^3.[29] Fortunately, the relative energy shift given in Fig. 9 depends only weakly on $\alpha_{0,I}$ and thus, calculations performed using either of the two different polarizability values give almost identical results for relative energy shift.

The nearly linear dependence of relative shift vs relative density calculated for the S–C model in Fig. 9 is only a weak function of the secondary parameters (solute and solvent polarizabilities and transition energies), although the slope of this dependence is somewhat more sensitive to the value of the hard sphere diameter σ. Since σ is calculated by the MSA[21] using the experimental values of density, dielectric constant, and polarizability of propane it may entail a relatively large error. Specifically, we have noticed that a small variation ($\sim 3\%$) in the value of polarizability used for calculating σ gives a relatively large ($\sim 15\%$) change in its calculated value. Subsequently, this changes the slope of the calculated relative energy shift such that the agreement with the experimental data is worse although still within the largest experimental error. This suggests that in order to compare the behavior of different solute–solvent systems, the parameters employed in the theory must be known quite well. In addition, highly accurate experiments are also essential in order to make such comparisons between a number of separate data sets and theoretical calculations.

VI. CONCLUSIONS

Optical absorption and emission spectra of the $^1B_{2u} \leftrightarrow {}^1A_{1g}$ transition of benzene dissolved in cryogenic propane are measured as a function of pressure, temperature and density. An interpretation of the experimentally monitored energy shifts and bandwidth dependences is suggested based on qualitative changes of the intermolecular potential in the ground and excited electronic states. The experimental results for the absorption energy shifts are compared to the theoretical calculations of the Onsager–Böttcher and Wertheim dielectric theories, as well as to the microscopic quantum statistical mechanical theory of Schweizer and Chandler.

Particular findings of the experimental study can be summarized as follows:

(1) Both absorption and emission spectral features exhibit red shifts with increasing pressure at constant temperature and blue shifts with increase of temperature at constant pressure. These shifts are linear functions of density (being both temperature and pressure dependent) and almost entirely cancel one another when the density is kept constant, i.e., temperature and pressure are simultaneously changed. This emphasizes the fundamental microscopic nature of density for the spectroscopic properties of benzene in solution, and indicates that pressure and temperature incre-

ments to the spectral behavior are of a comparable magnitude but cause opposite transition energy shifts. Several possible changes of the intermolecular potential surfaces can occur as a result of density (temperature and pressure) changes. The relative change of the energy gap between the ground and excited state potentials is argued to dominate and is presumably responsible for the observed transition energy shifts with density.

(2) Absorption half-widths increase with pressure but are independent of temperature, whereas emission half-widths exhibit asymmetric red-shaded broadening with both temperature and pressure. Interpretation of these experimental findings leads to the conclusion that the excited state potential surface is shifted with respect to the corresponding ground state potential in the intermolecular coordinate, and that the potential surface changes as a function of density; both repulsive and attractive parts of the potential are steeper, stronger functions of intermolecular distance at higher densities.

The experimental absorption shifts have been compared to the existing theories of solvent effects on solute electronic spectra. Specific results of the calculations are as follows:

(1) Classical, dielectric Onsager–Böttcher and Wertheim models predict qualitatively the red shift in transition energy but do not give the experimentally observed dependence of the relative shift as a function of density. Relatively good agreement of the modified O–B model with experiment is obtained by assuming (somewhat arbitrarily) that the inverse of the cube of cavity radius (R_u^{-3}) scales linearly with the density. The dielectric models are relatively simple but have the disadvantage that the spectral shift is entirely specified by solvent dielectric constant. The shift is thus not directly related to any microscopic parameter.

(2) The quantum statistical mechanical theory gives good agreement between the calculations of relative shifts and those found experimentally. Variations of the results due to a specific choice of parameters are generally relatively small and remain within the spread of the experimental data. Although this model predicts relative transition energy shifts it does not give the correct absolute value of the gas to liquid shift for the system studied. This limitation is a consequence of specific assumptions and was predicted by the authors of the model.

Our conclusions concerning the comparison of theory with experiment agree well with those of Schweizer and Chandler[12]; however, the present findings are based on new, reliable, and much more detailed experimental data. Pressure and density dependences of fluorescence as well as of the spectral bandwidths are reported for the first time. The bandwidths are not given by either the dielectric or quantum statistical mechanical models of solutions. The lack of the half-width dependence in the employed theoretical models is a limitation imposed by the mean field nature of the MSA and the assumption of the harmonic oscillator model for the fluctuating dipoles. Although theoretical analysis is limited to absorption data, our experimental results for emission suggest that the behavior of the relative shifts as a function of density is in both cases quite similar. The bandwidth dependences are slightly different for absorption and emission,

thus emphasizing the difference between the repulsive and attractive parts of the intermolecular potential.

Finally, we show that cryogenic liquid systems are very useful in the verification of liquid state theories: they allow relatively well resolved spectroscopic studies of dense liquids as a function of pressure, temperature, and density. Further studies should extend verification of the S–C model to different solute–solvent cryogenic systems; especially to those cryogenic liquids (N_2, CH_4, C_2H_6) which offer even narrower spectral bands and thus better resolution than propane. The only experimental limitations for employing high pressure in those systems may be solute solubilities and the liquid–solid lines of the low temperature liquids. Since most of the cryogenic liquids are characterized by relatively low critical temperatures, the supercritical regions of these liquids can be easily investigated experimentally. Such a study would be extremely interesting, since relatively little experimental and theoretical information exists for supercritical fluids.

ACKNOWLEDGMENTS

[1]E. R. Bernstein and J. Lee, J. Chem. Phys. **74**, 3159 (1981).
[2]M. W. Schauer, J. Lee, and E.R. Bernstein, J. Chem. Phys. **76**, 2773 (1982).
[3]F. Li, J. Lee, and E. R. Bernstein, J. Phys. Chem. **86**, 3606 (1982).
[4]F. Li, J. Lee, and E. R. Bernstein, J. Phys. Chem. **87**, 254 (1983).
[5]J. Lee, F. Li, and E. R. Bernstein, J. Phys. Chem. **87**, 260 (1983).
[6]F. Li, J. Lee, and E. R. Bernstein, J. Phys. Chem. **87**, 1175 (1983).
[7]J. Lee, F. Li, and E. R. Bernstein, J. Phys. Chem. **87**, 1180 (1983).
[8]For a review see, for example, A. T. Amos and B. L. Burrows, Adv. Quantum Chem. **7**, 289 (1973).
[9]R. L. Fulton, J. Chem. Phys. **61**, 4141 (1974).
[10]D. E. Sullivan and J. M. Deutch, J. Chem. Phys. **65**, 5315 (1976).
[11]The classical early papers are: (a) N.S. Bayliss, J. Chem. Phys. **18**, 292 (1950); (b) Y. Oshika, J. Phys. Soc. Jpn. **9**, 594 (1954); (c) E. G. McRae, J. Phys. Chem. **61**, 562 (1957); (d) H. C. Longuet-Higgins and J.A. Pople, J. Chem. Phys. **27**, 192 (1957).
[12]K. S. Schweizer and D. Chandler, J. Chem. Phys. **78**, 4118 (1983).
[13]A. Zipp and W. Kauzman, J. Chem. Phys. **59**, 4215 (1973).
[14]B. Y. Okamoto and H. G. Drickamer, J. Chem. Phys. **61**, 2870 (1974).
[15]B. Y. Okamoto and H. G. Drickamer, Proc. Natl. Acad. Sci. U.S.A. **71**, 4757 (1974).
[16]B. Y. Okamoto, W. D. Drotning, and H. G. Drickamer, Proc. Natl. Acad. Sci. U.S.A. **71**, 2671 (1974).
[17]W. M. Haynes and B. A. Younglove, in *Advances in Cryogenic Engineering* (Plenum, New York, 1982), Vol. 27.
[18]W. M. Haynes, J. Chem. Thermodyn. **15**, 419 (1983).
[19]R. D. Goodwin and W. M. Haynes, Natl. Bur. Stand. (U.S.) Monog. 170 (1982).
[20]L. Onsager, J. Am. Chem. Soc. **58**, 1486 (1936); C. J. F. Böttcher, *Theory of Electric Polarization* (Elsevier, Amsterdam, 1972).
[21]M. S. Wertheim, Mol. Phys. **25**, 211 (1973).
[22]D. Chandler, K. S. Schweizer, and P.G. Wolynes, Phys. Rev. Lett. **49**, 1100 (1982).
[23]G. S. Rushbrooke, G. Stell, and J. S. Hye, Mol. Phys. **26**, 1199 (1973).
[24]L. R. Pratt, Mol. Phys. **40**, 347 (1980).
[25]J. W. Eastman, J. Chem. Phys. **49**, 4617 (1968).
[26]W. P. Heiman, J. Chem. Phys. **51**, 354 (1969).
[27]C. S. Parmenter, Adv. Chem. Phys. **22**, 365 (1972).
[28]J. H. Callomon, T. M. Dunn, and I. M. Mills, Philos. Trans. R. Soc. London Ser. A **259**, 499 (1966).
[29]J. O. Hirschfelder, C. F. Curtiss, and R. B. Bird, *Molecular Theory of Gases and Liquids* (Wiley, New York, 1954).
[30]R. D. Levin and S. G. Lias, Natl. Stand. Ref. Data Ser., Natl. Bur. Stand. (U.S. GPO, Washington, D. C., 1982), Vol. 71.